Resonant triad interactions in a stably stratified uniform shear flow

Lima Biswas* and Priyanka Shukla†
Department of Mathematics, Indian Institute of Technology Madras, Chennai 600036, India

(Received 26 May 2020; accepted 26 January 2022; published 15 February 2022)

We investigate resonant triad interactions (RTIs) in a two-dimensional stably stratified uniform shear flow confined between two infinite parallel walls in the absence of viscous and diffusive effects. RTIs occur when three interacting waves satisfy the spatial and temporal resonance conditions of the form $\pm\boldsymbol{k}_m \pm \boldsymbol{k}_n = \boldsymbol{k}_r$ and $\pm\omega_m \pm \omega_n = \omega_r$ with $\boldsymbol{k}_{m,n,r}$ and $\omega_{m,n,r}$ being the wave vectors and frequencies of the interacting waves, respectively. In two-dimensional flows, the interaction between two primary modes having the same frequency ω but different wave numbers k_m and k_n produces two different secondary terms: one time-dependent (superharmonic) mode having frequency 2ω and wave number $k_m + k_n$, and the other time-independent mean flow with zero frequency and wave number $k_m - k_n$, where k_m and k_n are the horizontal components of the wave vectors $\boldsymbol{k}_m$ and $\boldsymbol{k}_n$, respectively. The linear stability problem is solved analytically, which gives the eigenfunctions in the form of modified Bessel functions. The differential equations governing the spatial amplitudes of the superharmonic mode and secondary mean flow are solved numerically as well as analytically using the spectral collocation method and the method of variation of parameters, respectively. It turns out that the linear operator associated with the differential equation of both secondary modes is the same as the linear stability operator and that the solvability condition of the differential equation is found to be associated with the existence of RTIs. We address two types of RTIs: self-resonances and different mode interactions. The self-resonating modes are identified using dispersion curves, but in different mode interactions the prediction of RTIs using dispersion curves is not so straightforward. Thus, to show the existence of RTIs for the different mode interaction case, we adopt a numerical method; in addition, we use the fact that the superharmonic mode diverges. Various cases of wave interactions in a stably stratified shear flow are analyzed in the presence of a resonant triad for various frequencies and mode numbers.

DOI: 10.1103/PhysRevFluids.7.023904

I. INTRODUCTION

Stratified flows are ubiquitous in nature, for instance, in lakes, rivers, oceans, and atmosphere, etc. With respect to gravity, stratification can be classified into two categories, namely, stable and unstable stratifications. The fluid is stably stratified if its density decreases (or is constant) with height and unstably stratified if, at least locally, its density increases with height. Such flows in bounded and unbounded geometries have been studied for decades [1–4]. In particular, stably stratified flows are of great interest from a geophysical point of view because of their ability to support the propagation of various kinds of gravity waves [5–8]. Notably, there are a number of instability induced phenomena associated with internal gravity waves, which are of interest from engineering as well as geophysical points of view; not all of them, however, are

*ma16d003@smail.iitm.ac.in
†priyanka@iitm.ac.in

fully understood at present [5,6,9]. One of the well-known phenomena associated with internal gravity waves in stably stratified flows is resonant triad interactions (RTIs) [10,11], which arise due to second-order nonlinear wave interactions satisfying the classical resonance conditions, namely, $\pm\boldsymbol{k}_m \pm \boldsymbol{k}_n = \boldsymbol{k}_r$ and $\pm\omega_m \pm \omega_n = \omega_r$, where $\boldsymbol{k}_{m,n,r}$ and $\omega_{m,n,r}$ are the wave vectors and frequencies of the interacting waves, respectively. It is worthwhile to note that RTIs—being the underlying energy transfer mechanism in internal gravity waves generated, for instance, by winds and tides in the ocean—play an important role in ocean related phenomena (tides, mixing, etc. [11]). If a small wave vector or frequency mismatch occurs in the condition of RTIs, i.e., $\boldsymbol{k}_r \pm \boldsymbol{k}_m \pm \boldsymbol{k}_n = \delta\boldsymbol{k}$ and $\omega_r \pm \omega_m \pm \omega_n = \delta\omega$, where $|\delta\boldsymbol{k}| \ll |\boldsymbol{k}_{m,n,r}|$ and $|\delta\omega| \ll |\omega_{m,n,r}|$, the interactions are referred to as near-resonant triad interactions, which have also been studied for several decades [12–14].

There are two significant consequences of RTIs: triadic resonance instability and superharmonic wave generation. In the former, one primary wave with wave vector $\boldsymbol{k}_0$ and frequency ω_0 generates two secondary waves with wave vectors $\boldsymbol{k}_\pm$ and frequencies $\omega_\pm$, and, owing to RTIs, continuous exchange of energy takes place among three waves [15,16]. In the latter, two primary waves having fixed equal frequency ω and wave vectors $\boldsymbol{k}_m$ and $\boldsymbol{k}_n$ generate a secondary superharmonic wave with frequency 2ω and wave vector $\boldsymbol{k}_m + \boldsymbol{k}_n$ [17,18]. Another interesting resonance triad phenomenon is the mean flow resonances [19], in which the secondary mean flow resonates with the background flow. These resonances appear when two primary waves of different wave vectors $\boldsymbol{k}_m$ and $\boldsymbol{k}_n$ with equal and opposite frequencies $\pm\omega$ interact and produce a spatially periodic mean flow with zero frequency ($\omega - \omega = 0$) and wave vector $|\boldsymbol{k}_m - \boldsymbol{k}_n|$.

The linear stability analysis forms a basic step for understanding wave interaction phenomena in stratified flows. The linear stability of stratified flows was initiated by Taylor [20] and Goldstein [21] where they conjectured that the sufficient condition for the stability of a heterogeneous shear flow is $\mathrm{Ri} > 0.25$, with Ri being the Richardson number (defined as the ratio of the squared buoyancy frequency to the square of vertical shear). The work of Taylor [20] was extended by Eliassen *et al.* [22], wherein the authors analyzed a stratified shear flow with a constant density gradient in a bounded geometry by formulating an initial value problem, and found that the flow is stable and unstable for $\mathrm{Ri} > 0$ and $\mathrm{Ri} < 0$, respectively. Their analysis revealed that for $\mathrm{Ri} > 0.25$ the system admits infinite number of discrete eigenvalues, whereas for $0 < \mathrm{Ri} < 0.25$ no discrete eigenvalue exists and the absolute of vertical and horizontal velocity disturbances decay asymptotically as t^{-1} and $t^{-0.5+\sqrt{0.25-\mathrm{Ri}}}$, respectively, where t is time. Furthermore, they identified that for $-0.75 < \mathrm{Ri} < 0$ the horizontal (vertical) component of velocity disturbance grows (decays) as $t^{-0.5+\sqrt{0.25-\mathrm{Ri}}}(t^{-1.5-\sqrt{0.25-\mathrm{Ri}}})$, and for $\mathrm{Ri} < -0.75$ at least one pair of discrete complex eigenvalues occur, thereby leading to exponentially growing disturbances.

Following Taylor's and Goldstein's works, Case [23] and Dyson [24] investigated the stability of stably stratified shear flows for $\mathrm{Ri} > 0$ in an idealized atmosphere by considering the inertial effects of the density in the flow. They showed that (i) the system contains one or more continuous spectra, and (ii) there exist an infinite number of discrete neutrally stable eigenvalues for $\mathrm{Ri} > 0.25$. Furthermore, Case [23] showed that the disturbance stream function decays as $t^{-0.5+\sqrt{0.25-\mathrm{Ri}}}$ using the asymptotic evaluation in the complex plane. Later, Brown and Stewartson [25] confirmed that the disturbance stream function varies as $t^{-1.5\pm\sqrt{0.25-\mathrm{Ri}}}$, which agrees with the result of Eliassen *et al.* [22]; however, it contradicts the results of Case [23]. For a comprehensive review, the reader is referred to Yaglom [26]. For $\mathrm{Ri} > 0.25$, the study by Booker and Bretherton [27] showed a significant energy transfer from internal waves to the background flow at the critical layer—a region where the phase velocity of the internal wave is the same as that of background flow. Later several studies considered resonant interactions near the critical layer; e.g., see Brown and Stewartson [25] and Grimshaw [28,29].

The theory of nonlinear wave interactions was introduced in the seminal work by Phillips [30], wherein he proved that second-order resonant interactions are not possible among three finite-amplitude surface gravity waves in deep water (in the absence of background shear) and that the cubic-order resonant interactions can occur among a group of four of such waves. These findings

were also confirmed experimentally by Longuet-Higgins [31]. Notwithstanding, RTIs exist among surface gravity waves in the presence of shear [32]. It may be noted that Refs. [30–32] consider a homogeneous (i.e., constant density) medium. Nonlinear wave interactions in a continuously stably stratified inviscid fluid in the absence of background shear (a heterogeneous medium with vertical anisotropy) were studied first by Thorpe [33], who proved the existence of RTIs among two surface waves and an internal gravity wave as well as among three internal gravity waves—provided that not all of them have the same mode number. A more generalized work that analyzes RTIs among internal gravity waves in a continuously stratified fluid in the presence of shear was carried out by Grimshaw [28]. He further extended this work to higher-order resonances [29]. Thus, the existence of RTIs among internal gravity waves in a continuously stratified shear flow is well established [28,29,33]. However, to the best of authors' knowledge, a weakly nonlinear analysis, which determines the control parameters rendering RTIs among internal gravity waves in a stratified shear flow, has not been reported so far. Therefore, the objective of this paper is to demonstrate a second-order weakly nonlinear analysis to investigate RTIs among internal gravity waves in an inviscid, continuously stratified shear flow. In particular, we focus on uniform shear (i.e., constant shear rate) in a stably stratified medium. The analysis leads to the second-order weakly nonlinear solution containing an arbitrary sum of the vertical modes at a fixed frequency to identify the existence of RTIs. Furthermore, we introduce a method to determine the control parameters for the existence of RTIs. The present study could prove useful for oceanic scenarios as the presence of shear flow (or any other mean flow) in a continuously stratified medium affects the energy transfer among different internal gravity wave harmonics as well as the energy transfer from the shear flow to each disturbance significantly [34,35].

The paper is organized as follows. The problem definition and non-dimensional equations are given in Sec. II. The linear stability problem and discussions on the analytical solution are studied in Sec. III. The nonlinear problem is discussed in Sec. IV. The first- and second-order solutions are given in Secs. IV A and IV B, respectively. The analytical solution for the second-order problem is formulated in Sec. IV C. The existence of resonant triad interactions among two primary waves having the same frequency ω and a superharmonic wave of frequency 2ω for self and non-self-resonant cases are presented in Sec. V, and our conclusions are in Sec. VI.

II. PROBLEM DEFINITION

Consider a two-dimensional stably stratified incompressible inviscid flow bounded between two oppositely moving solid walls at $z = \pm L$ with speed $\bar{U}_0$ along the x direction. The background flow under consideration is a parallel shear flow with constant shear rate, i.e.,

$$\bar{U}(z) = \bar{U}_0\, z/L, \tag{1}$$

in a stably stratified medium with density satisfying

$$\bar{\rho}(z) = \rho_m - \frac{1}{2}\rho_d \frac{z}{L}, \tag{2}$$

where ρ_m is a constant reference density and ρ_d is the density difference between top and bottom walls. The shear flow is superimposed in a background state such that the pressure $\bar{p}(z)$ and density $\bar{\rho}(z)$ are in hydrostatic balance:

$$\frac{\partial \bar{p}}{\partial z} = -g\bar{\rho}. \tag{3}$$

Note that the gradient of the background density is constant. To simplify the problem, we use the Boussinesq approximation, i.e., the density variation is negligible in the equations of motion except in the gravity term. Thus, the mass, internal energy, and momentum equations read

$$\nabla \cdot \boldsymbol{u} = 0, \qquad \frac{\partial \rho}{\partial t} + \boldsymbol{u} \cdot \nabla \rho = 0, \quad \text{and} \quad \rho_m \left(\frac{\partial}{\partial t} + \boldsymbol{u} \cdot \nabla \right) \boldsymbol{u} = -\nabla p + \rho \boldsymbol{g}, \tag{4}$$

where $\boldsymbol{u} = (u, w)$ is the velocity vector and ρ, p, and $\boldsymbol{g}$ are the density, pressure, and gravity fields, respectively.

A. Nonlinear disturbance equations

In order to find the disturbance equations, each of the flow variables is decomposed into its background state and infinitesimally small disturbance, such that,

$$\rho(x, z, t) = \bar{\rho}(z) + \rho'(x, z, t), \tag{5a}$$

$$p(x, z, t) = \bar{p}(z) + p'(x, y, t), \tag{5b}$$

$$[u(x, z, t), w(x, z, t)] = [\bar{U}(z) + u', w'], \tag{5c}$$

where the perturbations are denoted by a superscript prime. Substituting the above decomposition (5) into (4), we get the following disturbance equations:

$$\frac{\partial u'}{\partial x} + \frac{\partial w'}{\partial z} = 0, \tag{6a}$$

$$\left(\frac{\partial}{\partial t} + \bar{U}\frac{\partial}{\partial x}\right)\rho' = -w'\frac{\partial \bar{\rho}}{\partial z} - \left(u'\frac{\partial \rho'}{\partial x} + w'\frac{\partial \rho'}{\partial z}\right), \tag{6b}$$

$$\left(\frac{\partial}{\partial t} + \bar{U}\frac{\partial}{\partial x}\right)u' + \frac{d\bar{U}}{d\,z}w' = -\frac{1}{\rho_m}\frac{\partial p'}{\partial x} - \left(u'\frac{\partial u'}{\partial x} + w'\frac{\partial u'}{\partial z}\right), \tag{6c}$$

$$\left(\frac{\partial}{\partial t} + \bar{U}\frac{\partial}{\partial x}\right)w' = -\frac{1}{\rho_m}\frac{\partial p'}{\partial z} - \frac{g\rho'}{\rho_m} - \left(u'\frac{\partial w'}{\partial x} + w'\frac{\partial w'}{\partial z}\right). \tag{6d}$$

At the solid boundaries $z = \pm L$, the normal component of the velocity perturbation w' is zero, and the density perturbation ρ' is assumed to be zero. Taking the curl of momentum equations (6c)–(6d), and introducing the perturbation stream function ψ', we get

$$\left(\frac{\partial}{\partial t} + \bar{U}(z)\frac{\partial}{\partial x}\right)\nabla^2\psi' = \frac{g}{\rho_m}\frac{\partial \rho'}{\partial x} - \left(\frac{\partial \psi'}{\partial z}\frac{\partial}{\partial x} - \frac{\partial \psi'}{\partial x}\frac{\partial}{\partial z}\right)\nabla^2\psi', \tag{7}$$

where $u' = \partial\psi'/\partial z$, $w' = -\partial\psi'/\partial x$, and $\nabla^2 = \partial^2/\partial x^2 + \partial^2/\partial z^2$ is the Laplacian operator. Note that four disturbance equations (6a)–(6d) reduce to two equations (6b) and (7) for ρ' and ψ', respectively.

B. Nondimensional equations

For nondimensionalization, we use half of the gap between the walls, L, as a reference length scale, ρ_m as a reference density, the background flow speed at the wall, $\bar{U}_0$, as a reference velocity, and $L/\bar{U}_0$ as a reference timescale. We will use the same notation for the nondimensional variables, and here onward all the variables are in dimensionless form. The nondimensional disturbance equations read as

$$\left(\frac{\partial}{\partial t} + \bar{U}(z)\frac{\partial}{\partial x}\right)\rho' = -N^2\frac{\partial \psi'}{\partial x} + J(\psi', \rho'), \tag{8}$$

$$\left(\frac{\partial}{\partial t} + \bar{U}(z)\frac{\partial}{\partial x}\right)\nabla^2\psi' = \frac{gL}{\bar{U}_0^2}\frac{\partial \rho'}{\partial x} + J(\psi', \nabla^2\psi'), \tag{9}$$

where $\bar{U}(z) = z$, the dimensionless buoyancy frequency N is expressed as $N = \sqrt{-\frac{g}{\rho_m}\frac{d\bar{\rho}}{dz}}/\sqrt{\frac{g}{L}}$, and $J(f, g) = \frac{\partial f}{\partial x}\frac{\partial g}{\partial z} - \frac{\partial f}{\partial z}\frac{\partial g}{\partial x}$ is the Jacobian determinant. The dimensionless local Richardson number

Ri is defined as $\mathrm{Ri} = gLN^2/\bar{U}_0^2$. Rewriting (9) in terms of Ri, we get

$$\left(\frac{\partial}{\partial t} + \bar{U}(z)\frac{\partial}{\partial x}\right)\nabla^2\psi' = \frac{\mathrm{Ri}}{N^2}\frac{\partial \rho'}{\partial x} + J(\psi', \nabla^2\psi'). \tag{10}$$

Furthermore, eliminating the density gradient term of (10) using (8), we obtain

$$\left[\left(\frac{\partial}{\partial t} + \bar{U}(z)\frac{\partial}{\partial x}\right)^2\nabla^2 + \mathrm{Ri}\,\frac{\partial^2}{\partial x^2}\right]\psi' = \left(\frac{\partial}{\partial t} + \bar{U}(z)\frac{\partial}{\partial x}\right)J(\psi', \nabla^2\psi') + \frac{\mathrm{Ri}}{N^2}\frac{\partial J(\psi', \rho')}{\partial x}. \tag{11}$$

Note that Eqs. (8) and (11) form a coupled system of equations for unknowns ρ' and ψ'. The dimensionless boundary conditions are expressed as $\psi' = \rho' = 0$ at $z = \pm 1$. In the present paper, we focus on stably stratified linear density variations. Therefore N^2 and Ri are positive real constants. We shall consider different uniform stable stratifications by varying the dimensionless parameters (i) the buoyancy frequency N and (ii) the local Richardson number Ri.

III. LINEAR STABILITY THEORY

In the linear stability analysis, we neglect the nonlinear terms of disturbance equations and solve the resulting linear system by assuming the normal mode solution as

$$(\rho', \psi') = (\hat{\rho}(z), \hat{\psi}(z))e^{ik(x-ct)}, \tag{12}$$

where the hat over the quantity represents the complex amplitude, k is the streamwise wave number, and $c = c_r + i\,c_i$ is the complex phase velocity. The base flow is said to be stable, neutrally stable, or unstable if $k\,c_i < 0$, $k\,c_i = 0$, or $k\,c_i > 0$, respectively [36]. In the present study, we assume a positive wave number (i.e., $k > 0$), and thus the stability is determined by the sign of c_i. Neglecting the right-hand side nonlinear terms and substituting the normal mode solution (12) into (8) and (10), we get

$$(\bar{U} - c)\hat{\rho} = -N^2\,\hat{\psi}, \tag{13a}$$

$$(\bar{U} - c)\left(d_z^2 - k^2\right)\hat{\psi} = \frac{\mathrm{Ri}}{N^2}\,\hat{\rho}, \tag{13b}$$

where $d_z = d/dz$ and $d_z^2 = d^2/dz^2$. Eliminating density from (13b), we get

$$\left[(\bar{U} - c)^2\left(d_z^2 - k^2\right) + \mathrm{Ri}\right]\hat{\psi} = 0, \tag{14}$$

which is the modified Taylor-Goldstein equation [22] for the linear background shear flow with uniform stratification. The system of differential equations (13) or equivalently (14), along with the boundary conditions $\hat{\psi} = \hat{\rho} = 0$ at $z = \pm 1$, forms a generalized eigenvalue problem.

It is worth noticing that the linear stability problem (13) or (14) becomes singular when the background shear flow $\bar{U} = z \in [-1, 1]$ coincides with the phase velocity c of the perturbation, which leads to all continuous modes in the spectrum. The case of continuous modes is beyond the scope of the present study. Here the choice of $\mathrm{Ri} > 0.25$ is made, which ascertains that the system (13) possesses neutrally stable ($c_i = 0$) discrete modes [23], i.e., the eigenvalue c is real. Thus to avoid the singularity of (14) we assume that the phase speed c of interacting primary modes takes values either greater than 1 (forward propagating mode) or less than -1 (backward propagating mode). Due to the symmetry of the problem [37], it is sufficient to consider $c > 1$ in the present problem.

The two forward propagating primary modes having the same frequency ω may interact and produce the superharmonic with double frequency and the secondary mean flow with zero frequency. However, the focus of the present paper is the former one. For the sake of completeness the solution of the latter system is presented in Sec. IV C. Further analysis of RTIs involving two primary waves and a time-independent secondary mean flow is left for future.

A. Analytical solution and dispersion relation

The second-order differential equation (14) can be transformed into the modified Bessel equation [38]

$$Z^2 \frac{d^2\phi}{dZ^2} + Z \frac{d\phi}{dZ} - (Z^2 + \gamma^2)\,\phi = 0, \tag{15}$$

where $\hat{\psi}(z) = \sqrt{Z}\,\phi(Z)$, $Z = k\,(z - c)$, and $\gamma = \sqrt{0.25 - \mathrm{Ri}}$. In the present problem, $\mathrm{Ri} > 0.25$ everywhere in the flow domain, and therefore γ is always a purely imaginary number [22]. The general solution of the modified Bessel equation has the form

$$\phi(Z) = AI_\gamma(Z) + BK_\gamma(Z), \tag{16}$$

where A and B are two arbitrary constants, and $I_\gamma(Z)$ and $K_\gamma(Z)$ are the modified Bessel functions of order γ in variable Z; see Refs. [22,39] for more details. Consequently, the general solution of (14) reads

$$\hat{\psi}(z) = Af_1(z) + Bf_2(z), \tag{17}$$

where

$$f_1(z) = \sqrt{k(z-c)}I_\gamma(k(z-c)) \quad \text{and} \quad f_2(z) = \sqrt{k(z-c)}K_\gamma(k(z-c)), \tag{18}$$

are two linearly independent solutions of (14).

For finding the arbitrary constants A and B, we apply the boundary conditions $\hat{\psi}(\mp 1) = 0$ in the general solution (17), which give

$$AI_\gamma(k(-1-c)) + BK_\gamma(k(-1-c)) = 0 \quad \text{and} \quad AI_\gamma(k(1-c)) + BK_\gamma(k(1-c)) = 0. \tag{19}$$

The condition for the existence of nontrivial solutions of (19) yields the dispersion relation

$$\mathscr{D}(c,\, k;\, \mathrm{Ri}) = \begin{vmatrix} I_\gamma(k(-1-c)) & K_\gamma(k(-1-c)) \\ I_\gamma(k(1-c)) & K_\gamma(k(1-c)) \end{vmatrix} = 0, \tag{20}$$

or, in terms of frequency $\omega = c\,k$,

$$\mathscr{D}(\omega,\, k;\, \mathrm{Ri}) = \begin{vmatrix} I_\gamma(-k-\omega) & K_\gamma(-k-\omega) \\ I_\gamma(k-\omega) & K_\gamma(k-\omega) \end{vmatrix} = 0, \tag{21}$$

where $c \notin [-1, 1]$. It is verified that the dispersion relation remains invariant under the transformation $\omega \to -\omega$. Thus for each forward propagating mode with frequency ω there always exists a backward propagating mode with frequency $-\omega$ [37].

The linear system (19) has infinitely many solutions for A and B when the coefficients satisfy (20) or (21). From these infinite set of solutions we choose $A = K_\gamma(k(-1-c))$ and $B = -I_\gamma(k(-1-c))$. Finally substituting expressions of A and B into (17), we get

$$\hat{\psi}(z) = \sqrt{k(z-c)}[K_\gamma(k(-1-c))I_\gamma(k(z-c)) - I_\gamma(k(-1-c))K_\gamma(k(z-c))]. \tag{22}$$

Under the long-wavelength approximation (i.e., for $k = 0$), the phase speed c and the eigenfunction $\hat{\psi}(z)$ [given in (22)] can be expressed in a compact form [22,37]. However, for a general k, it is too cumbersome to obtain explicit expressions for c and $\hat{\psi}(z)$. Therefore, for nonzero k, we shall solve the dispersion relation (21) numerically in the following two ways: (i) for k by fixing ω, and (ii) for ω by fixing k, in the computer algebra software *Mathematica*. In the former, the obtained wave numbers at fixed ω are arranged in ascending order; i.e., mode 1, mode 2, ... have wave numbers $k_1, k_2, \ldots$, where $k_1 < k_2 \ldots$. In the latter, the obtained frequencies at fixed k are arranged in descending order, i.e., mode 1, mode 2, ... have frequencies $\omega_1, \omega_2, \ldots$ where $\omega_1 > \omega_2 \ldots$. In addition, the linear stability equations (13) are also solved numerically using the spectral collocation method [40], which gives eigenvalues ω for a fixed wave number k. Table I summarizes the roots $k_1, k_2, \ldots, k_8$ (arranged in ascending order) of the dispersion relation, which shows the presence of

TABLE I. The roots of the dispersion relation (21) for Ri = 5 showing the presence of different modes of wave numbers k_1 to k_8 for several frequencies.

$\omega \rightarrow$	1.09730	1.45442	1.61782	2.0197	2.12460	2.53705	2.626178	3.04056	3.12646	3.541166
k_1	0.721779	0.999998	1.13742	1.49994	1.59915	2.0	2.08802	2.5	2.58572	3.0
k_2	1.0	1.34115	1.5	1.89586	2.0	2.441	2.5	2.91411	3.0	3.41465
k_3	1.07379	1.42731	1.58973	1.99033	2.09508	2.50723	2.59633	3.01066	3.09657	3.51125
k_4	1.09172	1.44799	1.61116	2.01275	2.11762	2.52999	2.61912	3.03348	3.11939	3.53409
k_5	1.09598	1.4529	1.61625	2.01805	2.12295	2.53538	2.62451	3.03888	3.12479	3.53949
k_6	1.09699	1.45406	1.61745	2.01931	2.12422	2.53666	2.62578	3.04016	3.12607	3.54107
k_7	1.09723	1.45433	1.61773	2.01961	2.12452	2.53696	2.62608	3.04046	3.12637	3.54114
k_8	1.09729	1.45442	1.6178	2.01969	2.12459	2.537046	2.62616	3.04054	3.12645	3.54116

various internal modes of different wave numbers at a fixed frequency ω. It is seen from the last row of the table that k's are tending to ω.

Figure 1(a) illustrates the variation of the frequencies with the wave numbers of two forward propagating modes (mode 1 and mode 2). In Fig. 1(a), dots are the frequencies ω calculated from the dispersion relation (21), and the blue (red) line denotes numerically computed frequencies of the first (second) forward propagating mode obtained from the eigenvalue problem (13). It is seen that (i) numerically computed eigenvalues are in excellent agreement with those obtained from the dispersion relation, and (ii) the frequency increases with increasing wave number for each forward propagating mode. It is verified that the difference between frequencies of any two consecutive higher modes (mode 3, mode 4, and so on) is very small for any fixed wave number. The variation of corresponding phase speeds is also shown in Fig. 1(b). As mentioned earlier, we restrict ourselves to the modes with $c > 1$ ($\omega > k$). As $\omega \rightarrow k$ or $c \rightarrow 1$, the solution (22) of the linear problem (14) becomes invalid as it becomes singular due to the presence of a critical layer on the boundary. To find

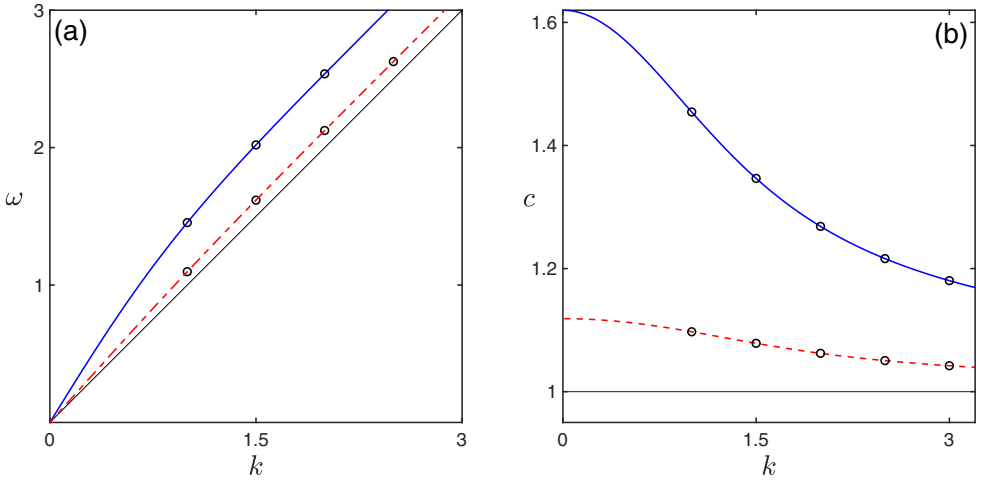

FIG. 1. Variation of the (a) frequency ω and (b) phase speed $c = \omega/k$ with the wave number k for Ri = 5. In panels (a) and (b), solid-blue and dashed-red lines correspond to the first and second forward propagating modes obtained from the eigenvalue problem (13), respectively, and circles represent the (ω, k) and (c, k) pairs obtained from the dispersion relation (21). The black solid lines on panels (a) and (b) denote $\omega = k$ and $c = 1$, respectively.

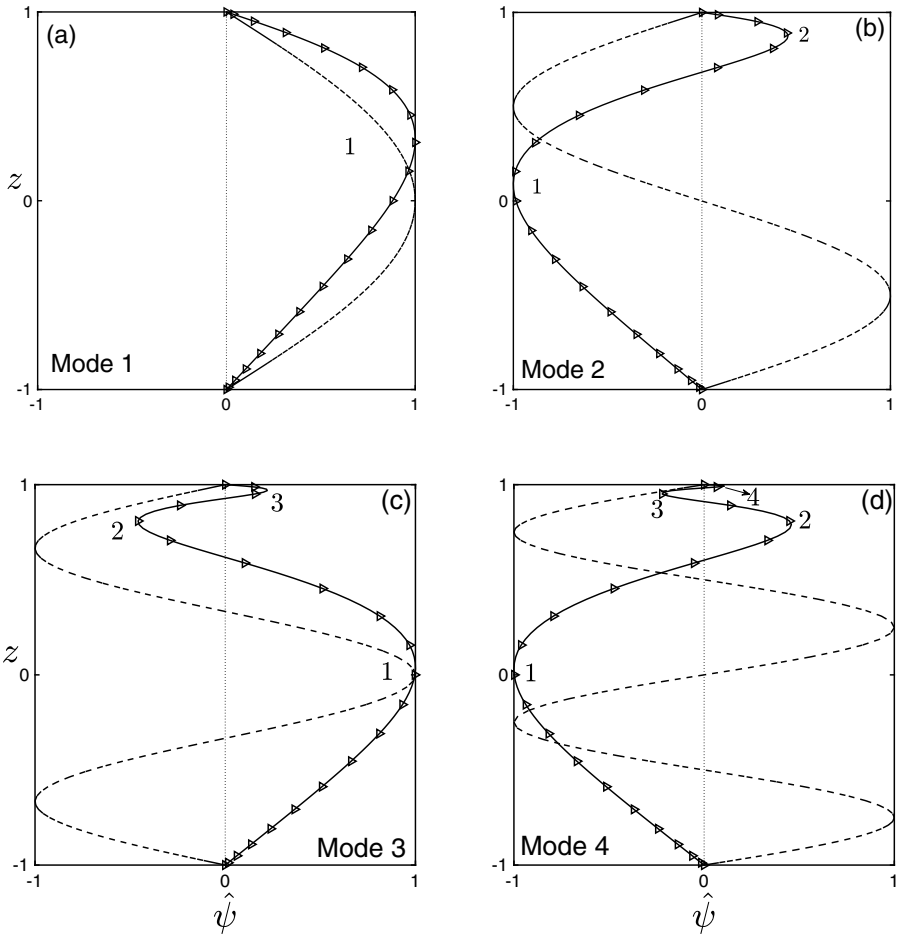

FIG. 2. Normalized eigenfunctions representing (a) mode 1, (b) mode 2, (c) mode 3, and (d) mode 4 for $\mathrm{Ri} = 5$ and $k = 1$. The solid and dashed lines denote analytical solutions in the presence and absence of shear, respectively; symbols refer to the numerical solution in the shear case.

a solution to the linear problem in the limit $\omega \to k$ (or $c \to 1$), one must consider the continuous spectra.

The variation of the first four eigenmodes of (14) with background shear (solid line) and without background shear (dashed line) for $k = 1$ and $\mathrm{Ri} = 5$ is depicted in Fig. 2. Here, symbols represent the numerically obtained eigenfunctions by solving (13), and the numbers in the panels indicate the extremities achieved by the eigenmode in the presence of shear flow. It is worth noticing that in the absence of shear flow the eigenmodes are nothing but the sine and cosine functions [5], which transform to the modified Bessel functions in the presence of uniform shear flow [22]; thus, the presence of uniform shear flow breaks the top-bottom symmetry of eigenmodes. The mode number of an eigenfunction is related to the number of zero-crossing as well as the number of extremum of the eigenfunction—if n is the mode number of the eigenmode, then the eigenmode becomes zero $n - 1$ times and achieves extremum n times between the domain $z \in (-1, 1)$. The eigenfunctions are asymmetric in the presence of background shear flow, which is in contrast to the no shear case where the eigenfunctions are symmetric or antisymmetric about the mid-depth; see Fig. 2. The shear flow also influences the frequency spectrum obtained from the nonlinear wave interactions. Notably, in the presence of vertical shear, the stably stratified flow admits transient growth [41,42] that originates either from the interaction of the edge waves [43] or the interactions of the members

of the continuous spectrum of the linear dispersion relation [44,45]. Moreover, shear flow is also responsible for shear-induced turbulent mixing and shear-induced breaking through the nonlinear wave interactions [46,47].

IV. WEAKLY NONLINEAR ANALYSIS

For examining the nonlinear problem, we use the regular perturbation expansion [48] in which the solution is expressed as an asymptotic power series in integer powers of a small parameter. Thus, we consider the solutions of (8) and (11) in the following power series form

$$(\psi',\ \rho') = \varepsilon\left(\psi^{(1)},\ \rho^{(1)}\right) + \varepsilon^2\left(\psi^{(2)},\ \rho^{(2)}\right) + \cdots, \tag{23}$$

where ε is a dimensionless small parameter, which quantifies the order of the amplitude of the perturbed stream function ψ', i.e., $\mathscr{O}(\varepsilon) \equiv \mathscr{O}(|\psi'|)$. In (23), the coefficients at $\mathscr{O}(\varepsilon)$ represent the plane wave solution of the linearized problem, and the higher order coefficients signify the nonlinear corrections due to the interactions among plane waves.

Substituting (23) into (8)–(11), and equating the coefficients of like powers in ε, we obtain a system of equations for $(\psi^{(n)},\ \rho^{(n)})$, which are solved successively. For instance, at $\mathscr{O}(\varepsilon)$, we obtain the linear disturbance equations [cf. (8) and (11)]

$$\mathscr{L}\,\psi^{(1)} = 0 \quad \text{and} \quad (\partial_t + \bar{U}\,\partial_x)\rho^{(1)} + N^2\,\partial_x\psi^{(1)} = 0, \tag{24}$$

where $\mathscr{L} = (\partial_t + \bar{U}\,\partial_x)^2\nabla^2 + \mathrm{Ri}\,\partial_{xx}$, and the subscripts x and t denote the respective derivatives. Similarly at $\mathscr{O}(\varepsilon^2)$, we get a second-order system for $\psi^{(2)}$ and $\rho^{(2)}$,

$$\mathscr{L}\,\psi^{(2)} = (\partial_t + \bar{U}\,\partial_x)J\left(\psi^{(1)},\ \nabla^2\psi^{(1)}\right) + \frac{\mathrm{Ri}}{N^2}\,\partial_x J\left(\psi^{(1)}, \rho^{(1)}\right), \tag{25a}$$

$$(\partial_t + \bar{U}\,\partial_x)\rho^{(2)} = -N^2\,\partial_x\psi^{(2)} + J\left(\psi^{(1)},\ \rho^{(1)}\right), \tag{25b}$$

where the right-hand side contains quadratic nonlinear terms involving the solutions of $\mathscr{O}(\varepsilon)$ problem.

A. First-order solution at $\mathscr{O}(\varepsilon)$

We write the first-order solution $(\psi^{(1)}, \rho^{(1)})$ as a superposition of waves with different wave numbers

$$\psi^{(1)} = \sum_j \psi_j(z)e^{i(k_j x - \omega_j t)} + \text{c.c.} \quad \text{and} \quad \rho^{(1)} = \sum_j \rho_j(z)e^{i(k_j x - \omega_j t)} + \text{c.c.}, \tag{26}$$

where $\omega_j = k_j c_j$ with $j \geqslant 1$ being a positive integer, and c.c. denotes the complex conjugate terms. Substituting (26) into (24), we get

$$L_j\psi_j(z) = 0 \quad \text{and} \quad \rho_j(z) = -N^2\frac{\psi_j(z)}{(\bar{U} - \omega_j/k_j)}, \tag{27}$$

where $L_j \equiv \mathscr{L}(\partial_t \to -i\omega_j, \partial_x \to ik_j, \partial_z \to d_z, \dots)$ is a complex differential operator, which is obtained by replacing the partial derivatives ∂_t, ∂_x, and ∂_z by $-i\omega_j$, ik_j, and d_z into the operator $\mathscr{L}$, respectively. As detailed in Sec. III, the exact solution of the first-order problem is expressed in terms of the modified Bessel function as

$$\psi_j(z) = \sqrt{p_j}[K_\gamma(-k_j - \omega_j)I_\gamma(p_j) - I_\gamma(-k_j - \omega_j)K_\gamma(p_j)], \tag{28}$$

where $p_j = k_j z - \omega_j$ and $\psi_j(\pm 1) = 0$; see (22).

B. Second-order solution at $\mathcal{O}(\epsilon^2)$ and three-wave interactions

Note that the right-hand side of the second-order system (25) is forced by the solution $(\psi^{(1)}, \rho^{(1)})$ of the first-order system. Owing to the forcing by primary (linear) waves, we can physically interpret the generation of harmonics (waves which are forced by linear waves); e.g., the two primary waves having the same frequency interact with each other, exchange energies, and give rise to the superharmonic and correction to the mean flow. These interacting waves form a resonance triad if the sums of their wave numbers and frequencies satisfy the resonance conditions,

$$\pm k_m \pm k_n = k_r \quad \text{and} \quad \pm \omega_m \pm \omega_n = \omega_r, \tag{29}$$

where k_m and k_n are the wave numbers of two interacting waves that produce a wave of wave number k_r with ω_m, ω_n, and ω_r being the corresponding frequencies.

In this paper, we consider the interaction between two primary modes of wave numbers k_m and k_n having the same frequency $\omega_m = \omega_n = \omega$ in two-dimensional Cartesian geometry. These two primary modes interact with each other and yield a superharmonic and a time-independent secondary mean flow with the wave number and frequency pairs as $(k_m + k_n, 2\omega)$ and $(k_m - k_n, 0)$, respectively. The superharmonic mode forms a resonant triad with two interacting primary modes when 2ω is one of the eigenvalues of (13) at wave number $k_m + k_n$, i.e., $(k_m + k_n, 2\omega)$ satisfies the dispersion relation $\mathscr{D}(2\omega,\ k_m + k_n;\ \mathrm{Ri}) = 0$. Similarly, the mean flow form a resonant triad with two interacting primary modes when 0 is one of the eigenvalues of the linearized problem (13) at wave number $k_m - k_n$, i.e., $(k_m - k_n, 0)$ satisfies the dispersion relation $\mathscr{D}(0,\ k_m - k_n;\ \mathrm{Ri}) = 0$. In other words, under the resonance condition, there exists a primary internal mode with wave number and frequency pair as $(k_m + k_n, 2\omega)$ or $(k_m - k_n, 0)$ in the system giving rise to a superharmonic and a time-independent secondary mean flow, respectively.

Substituting the expansion of $(\psi^{(1)}, \rho^{(1)})$ from (26) into (25), the right-hand side forcing terms of (25) can be expressed as

$$\sum_{m,n\geqslant 1} \left[A_{mn}(z)\, e^{i\,[(k_m+k_n)x - 2\,\omega\, t]} + B_{mn}(z)\, e^{i\,(k_m - k_n)x} + \text{c.c}\right], \tag{30}$$

where

$$\begin{aligned} A_{mn}(z) = (k_m + k_n)\Big[&- (\bar{U} - c_3)\left(k_m\, \psi_m \left(d_z^2 - k_n^2\right) d_z\psi_n - k_n\, d_z\psi_m \left(d_z^2 - k_n^2\right)\psi_n\right) \\ &+ \frac{\mathrm{Ri}}{N^2}\left(-k_m\, \psi_m\, d_z\rho_n + k_n\, \rho_n\, d_z\psi_m\right)\Big], \end{aligned} \tag{31a}$$

$$\begin{aligned} B_{mn}(z) = -(k_m - k_n)\Big[&\bar{U}\, k_m\, \psi_m \left(d_z^2 - k_n^2\right) d_z\psi_n + \bar{U}\, k_n\, d_z\psi_m \left(d_z^2 - k_n^2\right)\psi_n \\ &+ \frac{\mathrm{Ri}}{N^2}\left(k_m\, \psi_m\, d_z\rho_n - k_n\, \rho_n\, d_z\psi_m\right)\Big]. \end{aligned} \tag{31b}$$

The positive indices m and n are summed over all the primary wave numbers present in the system. Here, the phase velocity of the superharmonic mode is defined as $2\omega/(k_m + k_n)$. Note that the right-hand side forcing (30)–(31) arises due to the quadratic interaction between various modes present at the leading order. Consequently, the second-order solution $\psi^{(2)}$ has the same form as the two terms of the right-hand side forcing of (25a), thus the expression for $\psi^{(2)}$ reads

$$\psi^{(2)}(z) = \sum_{m,n\geqslant 1} \left[h_{mn}(z) e^{i[(k_m+k_n)x - 2\omega t]} + g_{mn}(z) e^{i(k_m - k_n)x} + \text{c.c.}\right]. \tag{32}$$

Substituting (32) into (25a) and equating the coefficients of $e^{i[(k_m+k_n)x - 2\omega t]}$ and $e^{i(k_m - k_n)x}$, we obtain equations for $h_{mn}(z)$ and $g_{mn}(z)$. For mode pair $(m,\ n)$, the spatial amplitudes of the superharmonic mode and the secondary mean flow are defined as $\bar{h}_{mn}(z) = h_{mn} + h_{nm}$ and $\bar{g}_{mn}(z) = g_{mn} + g_{nm}$, respectively. The equations governing $\bar{h}_{mn}(z)$ and $\bar{g}_{mn}(z)$ satisfy the following nonhomogeneous

differential systems:

$$L_2^+ \bar{h}_{mn}(z) = \bar{A}_{mn}(z), \tag{33}$$

$$L_2^- \bar{g}_{mn}(z) = \bar{B}_{mn}(z), \tag{34}$$

where $\bar{A}_{mn} = A_{mn} + A_{nm}$ and $\bar{B}_{mn} = B_{mn} + B_{nm}$ with A_{nm} and B_{nm} being obtained by interchanging m and n indices in the expressions of A_{mn} and B_{mn}, respectively; L_2^+ and L_2^- are the linear differential operators defined as

$$L_2^+ = -(-2\omega + \bar{U}(k_m + k_n))^2\left(d_z^2 - (k_m + k_n)^2\right) - \mathrm{Ri}\,(k_m + k_n)^2, \tag{35}$$

$$L_2^- = -\bar{U}^2(k_m - k_n)^2\left(d_z^2 - (k_m - k_n)^2\right) - \mathrm{Ri}\,(k_m - k_n)^2. \tag{36}$$

$\bar{h}_{mn}(z)$ and $\bar{g}_{mn}(z)$ satisfy the Dirichlet boundary condition, i.e., $\bar{h}_{mn}(\pm 1) = \bar{g}_{mn}(\pm 1) = 0$.

According to the Fredholm alternative theorem [49], exactly one of the statements holds. Either a nonhomogeneous system [(33) and (34)] has a unique solution, or the corresponding homogeneous system has a nontrivial solution. In the latter case, a nonhomogeneous system has no solution or infinitely many solutions, depending on whether the right-hand side is orthogonal to all nontrivial solutions of the corresponding adjoint homogeneous problem. For more details, see Sec. 8.7 of Ref. [49].

Specifically, the system $L_2^+ \bar{h}^h_{mn}(z) = 0$ has a nontrivial solution when 2ω is equal to one of the eigenvalues of the linear problem at wave number $k_m + k_n$. Moreover, the existence of a nontrivial homogeneous solution of (33) is exactly the case of resonant triad interaction (RTI), see (29), because there exist primary internal modes with frequency and wave number pair as (ω, k_m), (ω, k_n), and $(2\omega, k_m + k_n)$. Due to this fact, the divergence of $\bar{h}_{mn}(z)$ acts as an additional criterion for the existence of the RTIs in the superharmonic case.

Similarly, the solution of (34) diverges when the corresponding homogeneous system $L_2^- \bar{g}^h_{mn}(z) = 0$ has a nontrivial solution, the case when zero is one of the eigenvalues of the linear problem at wave number $k_m - k_n$. This is exactly the case of the RTIs because there exist linear modes with frequency and wave number pairs as (ω, k_m), (ω, k_n), and $(0, k_m - k_n)$. Similarly to $\bar{h}_{mn}(z)$, the divergence of $\bar{g}_{mn}(z)$ acts as an additional criterion for the existence of the mean flow resonance.

C. Analytical solution of $L_2^+ \bar{h}_{mn}(z) = \bar{A}_{mn}(z)$ and $L_2^+ \bar{g}_{mn}(z) = \bar{B}_{mn}(z)$ systems

We shall find the particular solution of (33) and (34) using the method of variation of parameters, which enables us to find the general solution of it. Let the general solution of the superharmonic system be

$$\bar{h}_{mn}(z) = C_1 f_1(z) + C_2 f_2(z) + f_1(z) u_1(z) + f_2(z) u_2(z), \tag{37}$$

where C_1 and C_2 are two arbitrary constants to be determined using the homogeneous boundary conditions at $z = \pm 1$. $\{f_1(z), f_2(z)\}$ forms a fundamental set of solutions of the corresponding homogeneous problem of (33), which is expressed in terms of the modified Bessel function of complex order $\gamma = \sqrt{0.25 - \mathrm{Ri}}$ as

$$f_1(z) = \sqrt{(k_m + k_n)\, z - 2\,\omega}\, I_\gamma[(k_m + k_n)z - 2\,\omega)],$$

$$f_2(z) = \sqrt{(k_m + k_n)\, z - 2\,\omega}\, K_\gamma[(k_m + k_n)z - 2\,\omega)], \tag{38}$$

and $u_1(z)$, $u_2(z)$ have the integral form

$$u_1(z) = -\int_{-1}^{z} \frac{f_2(\xi)\,\bar{A}_{mn}(\xi)}{[2\,\omega - (k_m + k_n)\,\zeta]^2\, W_h}\, d\xi, \quad u_2(z) = \int_{-1}^{z} \frac{f_1(\xi)\,\bar{A}_{mn}(\xi)}{[2\,\omega - (k_m + k_n)\,\xi]^2\, W_h}\, d\xi, \tag{39}$$

where $u_1(-1) = u_2(-1) = 0$ and $W_h = -(k_m + k_n)$ is the Wronskian of f_1 and f_2. In order to find the arbitrary constants, C_1 and C_2, we apply the Dirichlet boundary conditions $\bar{h}_{mn}(\mp 1) = 0$, which

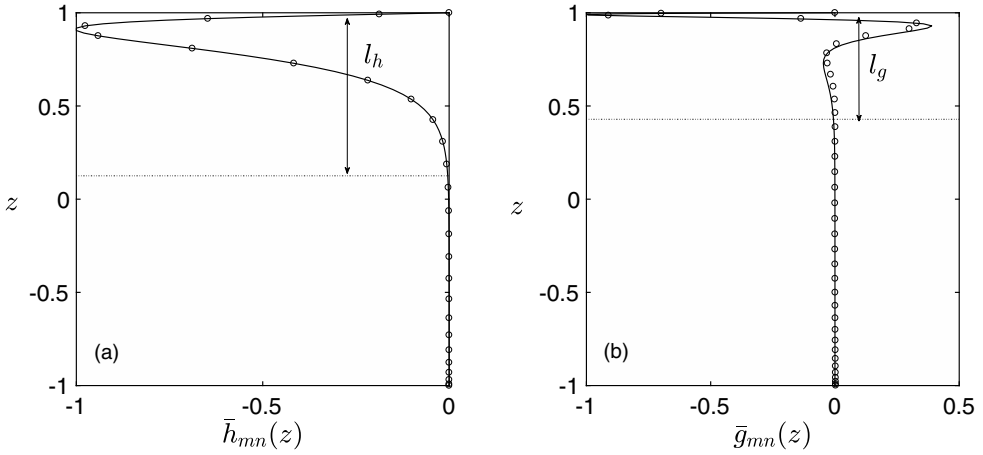

FIG. 3. The spatial amplitudes of (a) superharmonic mode ($\bar{h}_{mn}$) and (b) secondary mean flow ($\bar{g}_{mn}$). Solid line and circles denote the analytical [(42) and (43)] and numerical solutions [(33) and (34)], respectively.

give

$$\begin{aligned} C_1\, f_1(-1) + C_2\, f_2(-1) &= 0, \\ C_1\, f_1(1) + C_2\, f_2(1) + f_1(1)\, u_1(1) + f_2(1)\, u_2(1) &= 0. \end{aligned} \tag{40}$$

Solving the linear system (40), we obtain

$$C_1 = -C_2 \frac{f_2(-1)}{f_1(-1)} \quad \text{and} \quad C_2 = -\frac{f_1(-1)\,[\,f_1(1)\,u_1(1) + f_2(1)\,u_2(1)]}{-f_2(-1)\,f_1(1) + f_2(1)\,f_1(-1)}. \tag{41}$$

Finally, substituting C_1 and C_2 from (41) into (37) we obtain the analytical solution,

$$\begin{aligned} \bar{h}_{mn}(z) = {} & [\,f_1(1)\,u_1(1) + f_2(1)\,u_2(1)]\,[f_2(-1)\,f_1(z) - f_1(-1)\,f_2(z)] \\ & + [\,f_2(-1)\,f_1(1) + f_2(1)\,f_1(-1)]\,]\,f_1(z)\,u_1(z) + f_2(z)\,u_2(z)], \end{aligned} \tag{42}$$

where f_1, f_2 and u_1, u_2 are given by (38) and (39), respectively.

Similarly, analytical solution $\bar{g}_{mn}(z)$ of (34) is given by

$$\begin{aligned} \bar{g}_{mn}(z) = {} & [\,g_1(1)\,v_1(1) + g_2(1)\,v_2(1)]\,[g_2(-1)\,g_1(z) - g_1(-1)\,g_2(z)] \\ & + [\,g_2(-1)\,g_1(1) + g_2(1)\,g_1(-1)]\,[\,g_1(z)\,v_1(z) + g_2(z)\,g_2(z)], \end{aligned} \tag{43}$$

where g_1, g_2 and v_1, v_2 are defined as follows:

$$g_1(z) = \sqrt{(k_m - k_n)\,z}\, I_\gamma[(k_m - k_n)z] \quad \text{and} \quad g_2(z) = \sqrt{(k_m - k_n)\,z}\, K_\gamma[(k_m - k_n)z], \tag{44}$$

$$v_1(z) = -\int_{-1}^{z} \frac{g_2(\xi)\,\bar{B}_{mn}(\xi)}{[(k_m - k_n)\,\xi]^2\, W_g}\, d\xi \quad \text{and} \quad v_2(z) = \int_{-1}^{z} \frac{g_1(\xi)\,\bar{B}_{mn}(\xi)}{[(k_m - k_n)\,\xi]^2\, W_g}\, d\xi. \tag{45}$$

Here, $W_g = -(k_m - k_n)$ is the Wronskian of g_1 and g_2.

The calculations involved in the analytical solutions (42) and (43) are carried out with the help of the computer algebra software *Mathematica*. In addition, the second-order solutions are also computed numerically by solving directly (33) and (34) using a spectral collocation method [40] in MATLAB. For comparison purposes, we display the spatial amplitudes of superharmonic $\bar{h}_{mn}$ and secondary mean flow $\bar{g}_{mn}$ calculated numerically by solving (33) and (34) using 150 collocation points, and calculated from the analytical solutions (42) and (43), respectively, for $\mathrm{Ri} = 5$ and $\omega = 4.5128$; see Fig. 3. In panels (a) and (b), the characteristic lengths l_h and l_g of the superharmonic ($\bar{h}_{mn}$) and secondary mean flow ($\bar{g}_{mn}$), respectively, are marked by an arrow. The characteristic

length of superharmonic and secondary mean flow is defined as the depth where $\bar{h}_{mn}$ and $\bar{g}_{mn}$ vary significantly. Note that both $\bar{h}_{mn}$ and $\bar{g}_{mn}$ vary in a region close to the top wall, and the spatial amplitude of the superharmonic varies in a wider region in comparison to the secondary mean flow. It is clear from Fig. 3 that the analytical (solid line) and numerical (circles) solutions match excellently. Henceforth, we shall use the analytical solution for most of the results except for the three-dimensional visualization results shown in Fig. 5.

V. RESULTS

As described above, the main objective of the present paper is to determine the existence of RTIs among two primary modes at frequency ω and a superharmonic mode at frequency 2ω in a stably stratified uniform shear flow by analyzing interactions among the primary modes of varying frequencies.

For simplicity, we consider first four primary modes at a fixed frequency ω and label their wave numbers as k_1, k_2, k_3, and k_4; see Fig. 2. Here we shall investigate all possible interactions among any two of these modes of wave number k_m and k_n that form RTIs with the superharmonic mode h_{mn} generated by them, where $1 \leqslant m \leqslant n \leqslant 4$; thus we focus on the solution $\bar{h}_{mn}(z)$ of (33). In the following, we present results for two cases, namely, self-interaction ($m = n$) and different mode interaction ($m \neq n$).

A. Self-interaction $m = n$ ($1 \leqslant m = n \leqslant 4$)

Self-interactions occur when a primary mode interacts with itself. In this case, mode numbers of interacting modes are the same, i.e., $m = n$ and thus $k_m = k_n$ and $\omega_m = \omega_n$. The resonance conditions (29) reduce to

$$\frac{k_m}{k_r} = \pm\frac{1}{2} \qquad \text{and} \qquad \frac{\omega_m}{\omega_r} = \pm\frac{1}{2}, \tag{46}$$

where m and r are positive integers.

In a two-dimensional Cartesian geometry, self-interactions of primary modes are not possible in a uniformly stratified medium in the absence of shear. This is due to the fact that the Jacobian terms in the governing equations turn out to be zero [50]. However, in the presence of uniform shear Jacobian terms in Eq. (11) are non zero implying the possibility of the existence of self-resonating primary modes. Under the self-interactions, the spatial amplitude of the superharmonic mode satisfies the following equation:

$$L_2^+ \bar{h}_{mm}(z) = \bar{A}_{mm}(z), \tag{47}$$

where

$$L_2^+ \equiv -(-2\omega + 2\,k_m\bar{U})^2\left(d_z^2 - 4\,k_m^2\right) - 4\,\mathrm{Ri}\,k_m^2,$$

$$A_{mm} = 2\,k_m^2\left[-(\bar{U} - c_m)\left(\psi_m\left(d_z^2 - k_m^2\right)d_z\psi_m - d_z\psi_m\left(d_z^2 - k_m^2\right)\psi_m\right) + \frac{\mathrm{Ri}}{N^2}\left(\rho_m\, d_z\psi_m - \psi_m\, d_z\rho_m\right)\right].$$

Note that the frequencies and wave numbers are assumed to be positive. To find the existence of self-resonating modes, we need to find a $(k_m,\ \omega_m)$ pair satisfying the relations $\mathscr{D}(\omega_m, k_m; \mathrm{Ri}) = 0$ and $\mathscr{D}(2\omega_m, 2k_m; \mathrm{Ri}) = 0$ simultaneously.

Figures 4(a)–4(d) display the existence of self-resonances graphically for Ri = 30, 40, 50, and 60, respectively. In order to identify self-resonating modes, two graphs, $\omega(k)/k$ (solid lines) for the first four modes and $\omega(2k)/2k$ (dashed lines) for the first six modes, having the same abscissa k are depicted in Fig. 4. An intersection of a solid line and a dashed line represents a self-resonance point because $\omega/k = \omega(2k)/2k$, i.e., $\omega(k) = 2\omega(2k)$. For a given primary mode, the mode number of the resonating superharmonic mode can be determined from (4). The intersection patterns of dispersion curves of primary and superharmonic modes at wave numbers k and $2k$, respectively, suggest that the mode number of the superharmonic is less than or equal to $m - 1$.

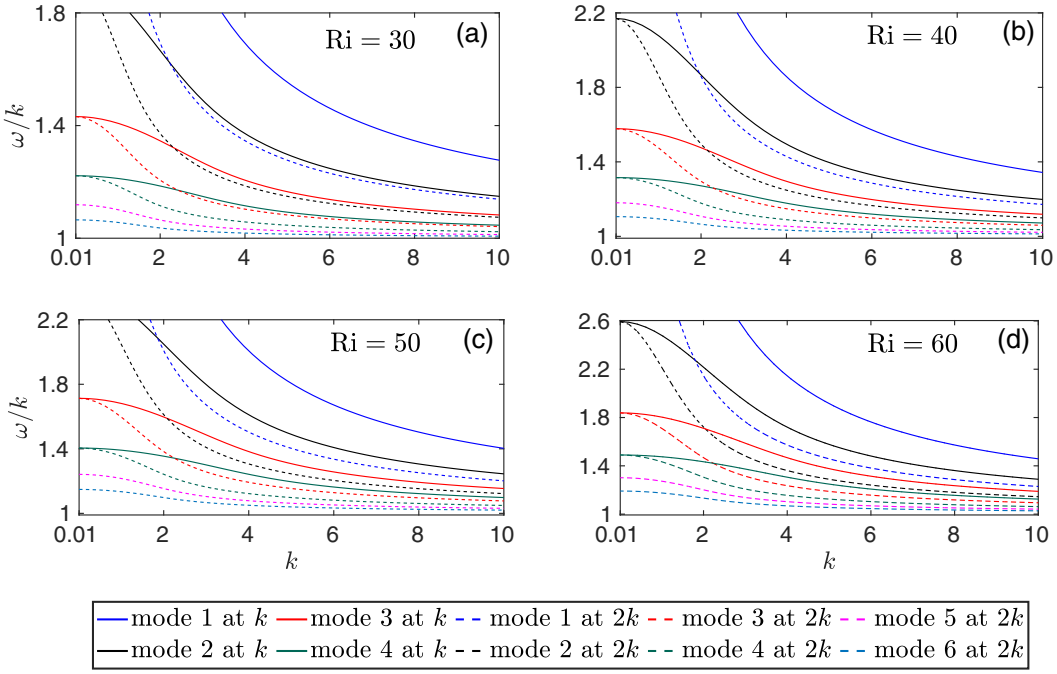

FIG. 4. Evidence of self-resonances for Ri = (a) 30, (b) 40, (c) 50, and (d) 60. In each panel, four solid lines from top to bottom denote the dispersion curves $\omega(k)/k$ as a function of k for modes 1–4, six dashed lines from top to bottom denote the dispersion curves $\omega(2k)/2k$ as a function of k for modes 1–6, and intersection points between a solid line and a dashed line represent the parameters k and ω satisfying the resonance condition (46).

B. Interactions among different modes $m \neq n$ ($1 \leqslant m < n \leqslant 4$)

For a broad range of Ri and ω, graphically finding out the resonance parameters for the interaction among two primary modes having the same frequency is not feasible. Nevertheless, we can adopt following numerical way based on the solutions of the dispersion relation, referred to as the mode search method.

Mode search method

(1) Generate $n_x \times n_y$ grid points on the (ω, Ri) plane and follow the following steps for each grid point.
(2) Generate a set $K_\omega = \{k \mid \mathscr{D}(\omega, k; \mathrm{Ri}) = 0\}$.
(3) Arrange K_ω in ascending order and label the elements as $k_1,\ k_2,\ k_3,\ k_4, \ldots$.
(4) Calculate $k_m + k_n$ for $k_m, k_n \in K_\omega$.
(5) Generate two sets:
  (a) $\Omega_{mn} = \{\omega \,|\, \mathscr{D}(\omega, k_m + k_n; \mathrm{Ri}) = 0\}$,
  (b) $K_{2\omega} = \{k \mid \mathscr{D}(2\omega, k; \mathrm{Ri}) = 0\}$.
(6) Corresponding to each $(m,\ n)$ pair define following sets:
  (a) $\Pi_\omega := \{\,|2\omega - \omega_r| \mid \omega_r \in \Omega_{mn}\}$,
  (b) $\Pi_k := \{\,|k_m + k_n - k_r^{2\omega}| \mid k_r^{2\omega} \in K_{2\omega}\}$.
(7) For each mode pair $(m,\ n)$ calculate the minimum of Π_ω and Π_k:
  (a) $\Delta_\omega = \min \Pi_\omega$ and the corresponding ω_r,
  (b) $\Delta_k = \min \Pi_k$ and the corresponding $k_r^{2\omega}$.
(8) If $\Delta_\omega = 0$, or equivalently $\Delta_k = 0$, there exist RTIs.

The condition for the existence of RTIs reduces to either $\Delta_\omega = 0$ or $\Delta_k = 0$. Note that the conditions $\Delta_\omega = 0$ or $\Delta_k = 0$ are equivalent since both these conditions imply that $(2\omega,\ k_m + k_n)$ satisfies the dispersion relation. However, due to the numerical limitations, achieving Δ_ω and Δ_k exactly zero is not possible. Thus, we say that RTIs exist if one of these two parameters is zero with some predefined accuracy specified by an error tolerance (Tol). By observing the values Δ_ω and Δ_k for various (ω, Ri) pairs, we fix $\mathrm{Tol} = 10^{-4}$, and RTIs exist if $|\Delta_\omega| \leqslant \mathrm{Tol}$ or $|\Delta_k| \leqslant \mathrm{Tol}$.

Without loss of generality, to study the interaction among two different modes ($m \neq n$, $1 \leqslant m < n \leqslant 4$) at the same frequency ω we assume that $n_x = 50$, $n_y = 80$, and $\omega \in [0.01, 5]$ and $\mathrm{Ri} \in [2, 10]$, which implies that the effect of buoyancy is much more than the effect of velocity shear.

Now we consider the interactions among two different modes with mode numbers m and n having the same frequency ω, and our aim is to find parameters Ri, ω, m, n for which RTIs exist. For different Richardson numbers (Ri), obtained by varying the density gradient, three waves satisfying the resonant conditions (29) with Tol are identified using the mode search method explained above, and the results are summarized in Table II. More precisely, at various Ri (first column) Table II displays the frequency ω (second column) with the corresponding wave numbers k_m and k_n (third and fourth columns) of two primary internal modes. As discussed above, at frequency ω these two interacting modes may or may not form a resonant triad with the third (superharmonic) mode. Table II also exhibits the resonating frequency ω_r (fifth column) and the resonating wave number $k_r^{2\omega}$ (sixth column) of the superharmonic mode, which forms a resonant triad with the primary modes of wave numbers k_m and k_n at frequency ω. The parameters Δ_k (seventh column) and Δ_ω (eighth column), defined as the wave number and frequency mismatch ($\Delta_k = |k_m + k_n - k_{2\omega}^r|$ and $\Delta_\omega = |2\omega - \omega_r|$), measure the accuracy in the resonance conditions (29) and tell us whether a resonant triad exists for the corresponding parameters or not. Note that for each mode pair Table II is arranged according to the ascending order of Δ_ω, i.e., the bold cells represent the parameters for which Δ_ω is the smallest. The last column of Table II shows the maximum absolute value of the second-order solution, i.e., $\max |\bar{h}_{mn}|$. Note that, at a resonating frequency ω_r, $\max |\bar{h}_{mn}|$ has a large value as compared to the neighboring nonresonating frequencies. It can be clearly seen from the parameters in bold in the table that RTIs exist for each listed mode pair $(m,\ n)$.

Resonance conditions can also be checked graphically without a prior knowledge of Δ_k or Δ_ω for given Ri and ω. In order to do so we first need to follow steps 2–5 of the mode search method to obtain the set Ω_{mn} for each mode pairs $(m,\ n)$. By plotting Ω_{mn} and the fixed point 2ω against $k_m + k_n$ the existence of RTIs can be concluded. RTIs occur if the point $(k_m + k_n, 2\omega)$ overlaps with any point of the set Ω_{mn}. As the exact values of Δ_ω and Δ_k are already mentioned in the table, to avoid repetition, we restrict from showing the existence of RTIs graphically here. However, the interested readers are referred to Fig. 4 of Ref. [51].

Divergence surface for $m \neq n$

So far, we have analyzed the evidence of RTIs for selected values of $(\omega,\ \mathrm{Ri})$ by the mode search method. However, for a wider range of parameters $(\omega,\ \mathrm{Ri})$, the mode search method is rather tedious. This can be avoided by directly using the fact that the second-order solution $\bar{h}_{mn}(z)$ diverges at the resonance point on $(\omega,\ \mathrm{Ri})$ plane.

Figure 5 shows the surface plot in the $(\omega,\ \mathrm{Ri},\ \log_{10} |\max \bar{h}_{mn}|)$ plane, where $\omega \in [0.01, 5]$ and $\mathrm{Ri} \in [2, 10]$ for each mode pair $(m,\ n)$. The color bar ranges from 0.5 (dark blue) to 9 (dark red). At the possible resonance locations of the $(\omega,\ \mathrm{Ri})$ plane, due to the divergence of $\bar{h}_{mn}(z)$, $\log_{10} |\max \bar{h}_{mn}|$ attains a large value as compared to the neighboring nonresonating points. Nevertheless, not all such $(\omega,\ \mathrm{Ri})$ values where $\log_{10} |\max \bar{h}_{mn}|$ achieves a large value correspond to RTIs. The large values or peaks in the surface plot may also appear due to numerical error. For all $(\omega,\ \mathrm{Ri})$ where $\bar{h}_{mn}(z)$ attains a large value, we check the resonance conditions (29) in order to confirm that RTIs exist or not.

By comparing panels (a)–(f) of Fig. 5 it is found that among all mode pairs $\max\limits_{1 \leqslant m < n \leqslant 4} \log_{10} |\max \bar{h}_{mn}|$ is attained when $(m,\ n) = (3, 4)$ for $(\omega,\ \mathrm{Ri}) = (2.61,\ 2)$; and for this

TABLE II. Richardson number, frequency, and wave numbers associated with resonance. For each $(m,\ n)$ pair, this table shows some parameters for RTIs predicted by Δ_ω or Δ_k. Parameters in bold correspond to minimum Δ_ω for each $(m,\ n)$ pair.

Ri	ω	k_m	k_n	ω_r	$k_r^{2\omega}$	Δ_k	Δ_ω	max $\lvert\bar{h}_{mn}\rvert$
				$(m,\ n) = (1,\ 2)$				
7.0	**1.4323**	**0.85033**	**1.2428**	**2.864505**	**2.09319**	$\mathbf{1\times10^{-4}}$	$\mathbf{6.7799\times10^{-5}}$	$\mathbf{2.1641\times10^{4}}$
7.0	4.21	3.4327	4.2098	8.4199	7.64265	1×10^{-4}	1.1151×10^{-4}	3.6693×10^{4}
7.0	4.31	3.5327	4.3098	8.6199	7.84265	1×10^{-4}	1.2691×10^{-4}	3.4419×10^{4}
5.5	4.21	3.6080	4.2098	8.4198	7.81803	2×10^{-4}	1.4440×10^{-4}	1.5948×10^{4}
5.5	4.31	3.7080	4.3098	8.6198	8.01803	2×10^{-4}	1.4890×10^{-4}	1.6888×10^{4}
5.5	4.41	3.8080	4.4098	8.8198	8.21803	2×10^{-4}	1.5200×10^{-4}	1.7954×10^{4}
				$(m,\ n) = (1,\ 3)$				
8.2	**4.51**	**3.599**	**4.5100**	**9.02000**	**8.10899**	$\mathbf{5\times10^{-6}}$	$\mathbf{9.2455\times10^{-7}}$	$\mathbf{5.6420\times10^{6}}$
7.0	4.21	3.4327	4.2100	8.42000	7.64265	4×10^{-5}	1.1922×10^{-6}	3.4336×10^{6}
8.2	4.61	3.6990	4.6100	9.21998	8.30899	5×10^{-6}	1.2925×10^{-5}	4.3073×10^{5}
7.0	4.31	3.5327	4.3100	8.61998	7.84265	4×10^{-5}	1.4208×10^{-5}	3.0954×10^{5}
8.2	4.71	3.7990	4.7100	9.41998	8.50899	5×10^{-5}	2.1125×10^{-5}	2.7950×10^{5}
				$(m,\ n) = (1,\ 4)$				
7.3	**4.21**	**3.3988**	**4.2099**	**8.42**	**7.60872**	$\mathbf{7\times10^{-8}}$	$\mathbf{5.2173\times10^{-8}}$	$\mathbf{8.0236\times10^{7}}$
7.9	4.51	3.6319	4.5100	9.02	8.14189	1×10^{-7}	1.2038×10^{-7}	4.3527×10^{7}
8.1	4.81	3.9099	4.8100	9.62	8.71992	2×10^{-5}	3.2267×10^{-7}	1.9454×10^{7}
5.5	4.31	3.7080	4.3100	8.62	8.01803	4×10^{-7}	4.0420×10^{-7}	6.2365×10^{6}
7.3	4.51	3.6987	4.5100	9.02	8.20872	1×10^{-6}	1.1522×10^{-6}	4.4685×10^{6}
				$(m,\ n) = (2,\ 3)$				
6.7	**4.21**	**4.2048**	**4.2096**	**8.41998**	**8.41482**	$\mathbf{4\times10^{-4}}$	$\mathbf{1.1682\times10^{-5}}$	$\mathbf{4.2440\times10^{6}}$
2.0	3.21	3.2086	3.2099	6.42001	6.40547	1×10^{-4}	1.3219×10^{-5}	3.5347×10^{6}
6.7	4.31	4.3048	4.3096	8.62002	8.61482	4×10^{-4}	2.2322×10^{-5}	1.8541×10^{6}
6.4	1.21	1.0594	1.1663	2.42004	2.22566	4×10^{-5}	3.6750×10^{-5}	1.5914×10^{5}
2.7	3.81	3.8055	3.8099	7.61996	7.61554	1×10^{-4}	3.6815×10^{-5}	5.0191×10^{6}
				$(m,\ n) = (2,\ 4)$				
2.2	**1.81**	**1.7910**	**1.8098**	**3.62**	**3.60081**	$\mathbf{1\times10^{-5}}$	$\mathbf{7.9970\times10^{-7}}$	$\mathbf{2.9213\times10^{7}}$
3.7	1.71	1.6431	1.7077	3.42	3.35087	7×10^{-5}	2.9214×10^{-6}	1.0153×10^{6}
5.1	1.71	1.5860	1.7028	3.42001	3.28873	7×10^{-5}	6.7562×10^{-6}	1.0676×10^{5}
3.6	3.41	3.3449	3.4100	6.81999	6.75485	5×10^{-5}	7.7865×10^{-6}	1.1579×10^{6}
3.6	3.51	3.4449	3.5100	7.01999	6.95485	5×10^{-5}	9.1866×10^{-6}	1.0185×10^{6}
				$(m,\ n) = (3,\ 4)$				
2.0	**2.61**	**2.6086**	**2.6099**	**5.22**	**5.21865**	$\mathbf{1\times10^{-4}}$	$\mathbf{6.4018\times10^{-8}}$	$\mathbf{4.4221\times10^{8}}$
2.0	2.71	2.7086	2.7099	5.42	5.41865	2×10^{-4}	4.5595×10^{-6}	6.9869×10^{6}
2.1	3.21	3.2083	3.2098	6.41999	6.41833	2×10^{-4}	4.7191×10^{-6}	8.2771×10^{6}
2.0	2.51	2.5086	2.5099	5.01999	5.01865	1×10^{-4}	5.1032×10^{-6}	4.8302×10^{6}
2.0	2.81	2.8086	2.8099	5.62001	5.61865	1×10^{-4}	8.1396×10^{-6}	4.3229×10^{6}

case the second-order solution $\bar{h}_{mn}(z)$ diverges, thereby leading to the possibility of resonant triad formation. Recall from Table II that for the above mentioned parameters, Δ_ω is indeed of order 10^{-8}, which also confirms the existence of RTIs. For mode pairs (1, 4) and (2, 4) [panels (c) and (e)], there exist several $(\omega,\ \mathrm{Ri})$ pairs for which $\log_{10}|\max \bar{h}_{mn}|$ attains large values, implying the possibility of RTIs at those points; see red peaks in panels (c) and (e). On the other hand, in the case of mode pair (1, 3), $|\max \bar{h}_{mn}|$ is very large [$\mathcal{O}(10^6)$] at two values of $(\omega,\ \mathrm{Ri})$, i.e., (4.51, 8.2) and (4.21, 7.0), as compared to their neighboring points; see panel (b). For these parameters, observing the values of Δ_ω and Δ_k from the corresponding rows of Table II one can conclude the occurrence

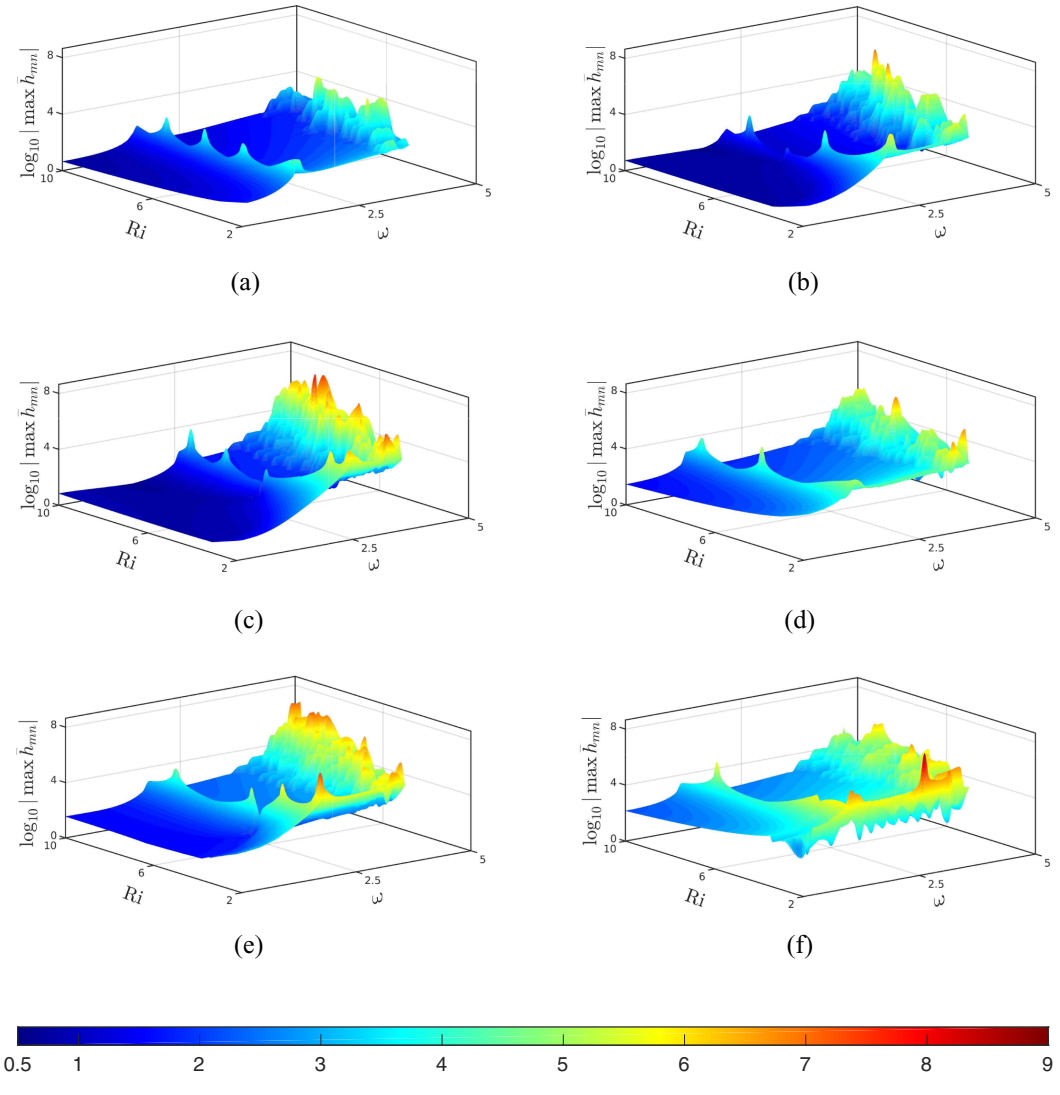

FIG. 5. The variation of $\log_{10} |\max \bar{h}_{mn}|$ in the (ω, Ri) plane for six mode pairs $(m,\ n)$: (a) $(1,\ 2)$, (b) $(1,\ 3)$, (c) $(1,\ 4)$, (d) $(2,\ 3)$, (e) $(2,\ 4)$, (f) $(3,\ 4)$.

of RTIs. Likewise, in the case of mode pair $(2,\ 3)$ we have obtained some additional $(\omega,\ \mathrm{Ri})$ values for which RTIs occur by observing $\log_{10} |\max\ \bar{h}_{mn}|$; see panel (d).

The above results show that for each considered mode pair, one can always define a minimum frequency $\omega = \omega_{\min}$ below which RTIs are not possible for any value of Richardson number (Ri) considered in the present analysis; see Table III. In other words, the operator L_2^+ is always non-singular for $\omega < \omega_{\min}$ and $\mathrm{Ri} \in [2, 10]$, that rules out the possibility of RTIs.

Thorpe [33] showed that RTIs among self-resonating modes $(m = n)$ are not possible in the absence of shear and that RTIs formed by the modes of mode numbers m and n must satisfy $\frac{1}{3} < \frac{m}{n} < 3$ with $m \neq n$. The present study confirms that self-resonances can occur in the presence of a constant background shear; see Sec. V A. It is verified that self-resonances $(m = n)$ develop at comparatively

TABLE III. Identified minimum frequencies below which RTIs are not possible for given mode pairs (m, n), $m \neq n$.

(m, n)	(1, 3)	(1, 4)	(2, 3)	(2, 4)	(3, 4)
$\omega_{\min}$	1.91	2.41	1.21	1.71	0.01

higher Ri than the interactions among two different modes ($m \neq n$). In self-resonance, the mode number of resonating superharmonic mode is found to be less than or equal to $m - 1$, with m being the mode number of the primary mode (see Fig. 4). In contrast, in the different mode interaction case (i.e., when $m \neq n$), the mode number of the resonating superharmonic mode cannot be predicted from the mode numbers m and n of the primary modes in the constant shear case; nevertheless, in this case, the mode number of the superharmonic wave can be calculated by counting the number of local extrema in the variation of spatial amplitudes. It should be noted that for uniformly stratified system with no background current, the mode number of the resonating superharmonic mode equals $m - n$ with m and n being the mode numbers of the primary modes [33].

VI. CONCLUSION

This paper has discussed the interaction of internal gravity waves in a two-dimensional stably stratified uniform shear flow bounded between two infinite horizontal parallel plates. In particular, we have focused on resonant triad interactions (RTIs) among two primary modes of the same frequency ω and a superharmonic mode of frequency 2ω. Various waves have been determined using the analytical solution by finding wave numbers for a specified wave frequency or vice versa. Furthermore, these calculated values have also been verified numerically by solving an eigenvalue problem. The existence of a resonance triad has been found to be associated with the divergence of the superharmonic mode $\bar{h}_{mn}(z)$. The superharmonic mode diverges when any of the following two conditions are satisfied: (i) $(2\omega, k_m + k_n)$ satisfies the dispersion relation, and (ii) the right-hand side $\bar{A}_{mn}(z)$ of (33) is nonorthogonal to the adjoint eigenfunction associated with the homogeneous problem. While the first condition is the standard resonance triad condition (29), the other is the Fredholm alternative [49]. It has been established that for a given (m, n) mode pair, the resonance conditions are indeed met at some specific peaks—referred to as diverging second-order solutions—of the surface plot in the $(\omega, \mathrm{Ri}, \log_{10} |\max \bar{h}_{mn}|)$ plane. These peaks are generated due to the divergence of the spatial amplitude $\bar{h}_{mn}(z)$ of superharmonic mode, implying the existence of resonance triads. Following the same analysis for finding the parameters for RTIs in the superharmonic case, the existence of mean flow resonances can be analyzed. For mean flow resonances $(0, k_m - k_n)$ must satisfy the dispersion relation, i.e., $\mathscr{D}(0, k_m - k_n; \mathrm{Ri}) = 0$. This analysis is beyond the scope of the present work and is left for the future.

In the present work, the existence of RTIs in the presence of uniform background shear and linear stable stratification has been studied. For various local Richardson numbers Ri and frequencies ω, the existence of RTIs involving the primary modes of mode numbers m and n with frequency ω, and the superharmonic mode formed by these, have been explored. The results have been shown for two cases: self-resonance ($m = n$) interaction and interaction between different modes ($m \neq n$). Note that self-resonances are not possible in a uniformly stratified system in the absence of shear. However, self-resonance may occur in a nonuniformly stratified system without any background shear flow [5]; for instance, under Earth's rotation, the existence of RTIs among primary internal modes in a nonuniformly stratified system has been reported in Ref. [18]. In the present scenario, i.e., a uniformly stratified system with uniform background shear, it has been observed that self-resonances occur at higher Ri than different mode interactions ($m \neq n$). For each Ri considered in this paper, it has been observed that the self-resonance interactions of primary mode 1 are not possible, but self-resonances occur for each primary mode with mode numbers $m = 2$, 3, and 4.

By observing the intersection patterns of dispersion curves for primary modes and their second harmonics from Fig. 4, it can be concluded that the mode numbers of the corresponding resonating superharmonics are less than or equal to $m-1$ for each of these primary modes. The wave numbers and frequencies of the self-resonating modes have been determined by plotting the dispersion relation. In contrast, finding the existence of RTIs by plotting the dispersion relation is tedious in the case of interactions among different modes ($m \neq n$). Thus we use the fact that superharmonic mode diverges at a resonance point to find the resonance points in this case.

To find the resonance parameters for a wider range of Ri and ω, we have developed a numerical technique. It turns out that the criteria for the existence of RTIs involving the modes m and n having frequency ω are $\Delta_k = |k_m + k_n - k_r^{2\omega}| = 0$ or $\Delta_\omega = |2\,\omega - \omega_r| = 0$. Notably, $\bar{h}_{mn}(z)$ diverges when Δ_k and Δ_ω are exactly zero, which is when the associated homogeneous equation has a nontrivial solution. Note that zero Δ_k and zero Δ_ω cannot be ascertained in the numerical solutions. Thanks to the above fact, we could find the solution $\bar{h}_{mn}(z)$ and hence an integer r to determine $k_r^{2\omega}$ as well as ω_r. In contrast to the mode search method based only on the triad conditions, the superharmonic solution $\bar{h}_{mn}(z)$ allows us to determine the positions of resonance triads for the full range of parameters (ω, Ri) more efficiently. Note that the present nonlinear problem has been tackled analytically and verified numerically. The evidence of resonant triads gives us an understanding of the energy transfer among modes of different wave numbers. The present work can be extended towards more realistic velocity and stratification profiles commonly seen in nature, for instance, (i) ocean-like stratification profiles where the density increases rapidly with depth in a pycnocline region [52], and (ii) estuarine velocity profiles where the part closer to the free surface is analogous to a shear flow and the part near the bottom boundary is analogous to boundary layer profile [53]. RTIs in critical layers (where the disturbance phase speed coincides with the background flow velocity) can also be an interesting extension of the present study. Moreover, the present study could serve as a benchmark for several other stratified flow problems, for instance, multilayer stratified flows, compressible stratified flows, etc.

ACKNOWLEDGMENTS

The authors gratefully acknowledge the anonymous reviewers and the editor Prof. Bruce Sutherland for their valuable suggestions. The authors also thank Prof. Manuel Torrilhon, Dr. Vinay Kumar Gupta, and Dr. Anubhab Roy for inspiring discussions at the early stages of this work. P.S. acknowledges IIT Madras for a New Faculty Seed Grant (MAT/1617/671/NFSC/PRIY).

[1] C. Yih, Stratified flows, Annu. Rev. Fluid Mech. **1**, 73 (1969).
[2] T. H. Bell, Lee waves in stratified flows with simple harmonic time dependence, J. Fluid Mech. **67**, 705 (1975).
[3] R. Grimshaw, *Environmental Stratified Flows* (Springer, New York, 2002).
[4] W. R. Peltier and C. P. Caulfield, Mixing efficiency in stratified shear flows, Annu. Rev. Fluid Mech. **35**, 135 (2003).
[5] B. R. Sutherland, *Internal Gravity Waves* (Cambridge University Press, Cambridge, 2010).
[6] J. S. Turner, *Buoyancy Effects in Fluids* (Cambridge University Press, Cambridge, 1973).
[7] J. Lighthill, *Waves in Fluids* (Cambridge University Press, Cambridge, 2001).
[8] D. E. Loper, *Geophysical Waves and Flows: Theory and Applications in the Atmosphere, Hydrosphere and Geosphere* (Cambridge University Press, Cambridge, 2017).
[9] C. Staquet and J. Sommeria, Internal gravity waves: From instabilities to turbulence, Annu. Rev. Fluid Mech. **34**, 559 (2002).
[10] A. D. Craik, *Wave Interactions and fluid Flows* (Cambridge University Press, Cambridge, 1988).
[11] P. Müller, G. Holloway, F. Henyey, and N. Pomphrey, Nonlinear interactions among internal gravity waves, Rev. Geophys. **24**, 493 (1986).

[12] D. J. Benney, Non-linear gravity wave interactions, J. Fluid Mech. **14**, 577 (1962).
[13] C. R. Koudella and C. Staquet, Instability mechanisms of a two-dimensional progressive internal gravity wave, J. Fluid Mech. **548**, 165 (2006).
[14] K. G. Lamb, Tidally generated near-resonant internal wave triads at a shelf break, Geophys. Res. Lett. **34**, L18607 (2007).
[15] B. R. Sutherland and R. Jefferson, Triad resonant instability of horizontally periodic internal modes, Phys. Rev. Fluids **5**, 034801 (2020).
[16] T. Dauxois, S. Joubaud, P. Odier, and A. Venaille, Instabilities of internal gravity wave beams, Annu. Rev. Fluid Mech. **50**, 131 (2018).
[17] S. Wunsch, Harmonic generation by nonlinear self-interaction of a single internal wave mode, J. Fluid Mech. **828**, 630 (2017).
[18] D. Varma and M. Mathur, Internal wave resonant triads in finite-depth non-uniform stratifications, J. Fluid Mech. **824**, 286 (2017).
[19] R. H. J. Grimshaw, The modulation of an internal gravity-wave packet, and the resonance with the mean motion, Stud. Appl. Math. **56**, 241 (1977).
[20] G. I. Taylor, Effect of variation in density on the stability of superposed streams of fluid, Proc. R. Soc. A **132**, 499 (1931).
[21] S. Goldstein, On the stability of superposed streams of fluids of different densities, Proc. R. Soc. A **132**, 524 (1931).
[22] A. Eliassen, E. Høiland, and E. Riis, *Two-dimensional Perturbation of a Flow with Constant Shear of a Stratified Fluid, Institute of Theoretical Astrophysics* (Norwegian Academy of Science and Letters, Oslo, 1953).
[23] K. M. Case, Stability of an idealized atmosphere. I. Discussion of results, Phys. Fluids **3**, 149 (1960).
[24] F. J. Dyson, Stability of an idealized atmosphere. II. Zeros of the confluent hypergeometric function, Phys. Fluids **3**, 155 (1960).
[25] S. N. Brown and K. Stewartson, On the nonlinear reflexion of a gravity wave at a critical level. Part 1, J. Fluid Mech. **100**, 577 (1980).
[26] A. M. Yaglom, *Hydrodynamic Instability and Transition to Turbulence*, Fluid Mechanics and Its Applications Vol. 100 (Springer, Dordrecht, 2012).
[27] J. R. Booker and F. P. Bretherton, The critical layer for internal gravity waves in a shear flow, J. Fluid Mech. **27**, 513 (1967).
[28] R. Grimshaw, Resonant wave interactions in a stratified shear flow, J. Fluid Mech. **190**, 357 (1988).
[29] R. Grimshaw, Resonant wave interactions near a critical level in a stratified shear flow, J. Fluid Mech. **269**, 1 (1994).
[30] O. M. Phillips, On the dynamics of unsteady gravity waves of finite amplitude Part 1. The elementary interactions, J. Fluid Mech. **9**, 193 (1960).
[31] M. S. Longuet-Higgins, Resonant interactions between two trains of gravity waves, J. Fluid Mech. **12**, 321 (1962).
[32] A. D. D. Craik, Resonant gravity-wave interactions in a shear flow, J. Fluid Mech. **34**, 531 (1968).
[33] S. A. Thorpe, On wave interactions in a stratified fluid, J. Fluid Mech. **24**, 737 (1966).
[34] V. V. Voronovich, D. E. Pelinovsky, and V. I. Shrira, On internal wave-shear flow resonance in shallow water, J. Fluid Mech. **354**, 209 (1998).
[35] H. Chen and Q. Zou, Effects of following and opposing vertical current shear on nonlinear wave interactions, Appl. Ocean Res. **89**, 23 (2019).
[36] P. G. Drazin and W. H. Reid, *Hydrodynamic Stability*, Cambridge Mathematical Library, 2nd ed. (Cambridge University Press, Cambridge, 2004).
[37] A. Davey and W. H. Reid, On the stability of stratified viscous plane Couette flow. Part 1. Constant buoyancy frequency, J. Fluid Mech. **80**, 509 (1977).
[38] M. Abramowitz and I. A. Stegun, *Handbook of Mathematical Functions with Formulas, Graphs, and Mathematical Tables* (U.S. GPO, Washington, 1964), Vol. 55.
[39] L. Engevik, A note on a stability problem in hydrodynamics, Acta Mech. **12**, 143 (1971).

[40] C. Canuto, M. Hussaini, A. M. Quarteroni, and T. A. Zang, *Spectral Methods in Fluid Dynamics* (Springer-Verlag, Berlin, 1988).
[41] P. J. Schmid and D. S. Henningson, *Stability and Transition in Shear Flows* (Springer, Berlin, 2001).
[42] E. G. Iliakis and N. A. Bakas, Linear non-modal growth of planar perturbations in a layered Couette flow, Fluids **6**, 442 (2021).
[43] A. Guha and G. A. Lawrence, A wave interaction approach to studying non-modal homogeneous and stratified shear instabilities, J. Fluid Mech. **755**, 336 (2014).
[44] K. M. Case, Stability of inviscid plane Couette flow, Phys. Fluids **3**, 143 (1960).
[45] C. C. Lin, Some mathematical problems in the theory of the stability of parallel flows, J. Fluid Mech. **10**, 430 (1961).
[46] S. Lewin and C. Caulfield, The influence of far field stratification on shear-induced turbulent mixing, J. Fluid Mech. **928**, A20 (2021).
[47] C. J. Howland, J. R. Taylor, and C. Caulfield, Shear-induced breaking of internal gravity waves, J. Fluid Mech. **921**, A24 (2021).
[48] A. H. Nayfeh, *Perturbation Method* (Wiley-VCH, Weinheim, 2000).
[49] E. Kreyszig, *Introductory Functional Analysis with Applications* (Wiley, New York, 1978).
[50] P. Husseini, D. Varma, T. Dauxois, S. Joubaud, P. Odier, and M. Mathur, Experimental study on superharmonic wave generation by resonant interaction between internal wave modes, Phys. Rev. Fluids **5**, 074804 (2020).
[51] L. Biswas and P. Shukla, Stability analysis of a resonant triad in a stratified uniform shear flow, Phys. Rev. Fluids **6**, 014802 (2021).
[52] A. E. Gill, *Atmosphere-Ocean Dynamics* (Elsevier, Amsterdam, 2016).
[53] P. MacCready and W. R. Geyer, Advances in estuarine physics, Annu. Rev. Marine Sci. **2**, 35 (2010).